ARTICLE

Ion Distribution in Electrified Micropores and Its Role in the Anomalous Enhancement of Capacitance

Guang Feng,[†] Rui Qiao,[†,*] Jingsong Huang,[‡] Bobby G. Sumpter,[‡] and Vincent Meunier[‡,*]

[†]College of Engineering & Science, Clemson University, Clemson, South Carolina 29634-0921 and [‡]Oak Ridge National Laboratory, Bethel Valley Road, Oak Ridge, Tennessee 37831-6367

ABSTRACT The distribution of K^+ ions in electrified slit-shaped micropores with pore widths ranging from 9.36 to 14.7 Å was studied using molecular dynamics simulations. We show that, in slit pores with pore widths between 10 and 14.7 Å, the K^+ ion distribution differs qualitatively from that described by classical electrical double-layer (EDL) theories in that fully hydrated K^+ ions accumulate primarily in the central plane of the slit pores. This phenomenon disappears when the pore width is narrower than 10 Å. Ion hydration and water−water interactions, which are rarely considered in prior EDL theories for micropores, are found to be responsible for this behavior. On the basis of these results, we have developed a new sandwich capacitance model to describe the capacitance of the EDLs formed by K^+ ions enclosed in slit-shaped micropores. This model is capable of predicting the anomalous enhancement of capacitance experimentally observed in micropores.

KEYWORDS: electrochemical capacitor · electrical double layer · micropore · ion hydration · sandwich model

Electrical energy storage plays a critical role in many high-profile energy technologies such as generation of electricity from renewable sources and as key components of all-electric vehicles.[1] Electrochemical capacitors (ECs) use the electric field in the electrical double layers (EDLs) established at the electrode/electrolyte interfaces to store electrical energy.[2] Because of their high power density and excellent cyclability, ECs are emerging as an ideal solution for many electrical energy storage applications.[3−5] The primary limitation of ECs is their moderate energy density, which is typically less than 10 Wh/kg. To address this limitation, electrodes with high specific surface area have been developed. In particular, electrodes featuring micropores (pore size <20 Å) are increasingly being used, and impressive improvement in energy density has been made recently.[4] However, current knowledge of the EDLs in micropores is still rudimentary, and many experimental observations remain poorly understood. For example, the area-normalized capacitance of activated carbon electrodes immersed in 6 M KOH solution has been found to increase from ~6 μF/cm^2 to ~12 μF/cm^2 as the mean pore size of the electrode decreases from 14.5 to 10.6 Å.[6] A similar anomalous enhancement has also been reported previously for micropores in organic electrolytes and in room-temperature ionic liquids.[7,8] Such an anomalous enhancement cannot be explained even qualitatively by the classical EDL theories based on the Poisson−Boltzmann (PB) equation.[9,10]

To rationalize the anomalous enhancement of capacitance in micropores, an electric wire-in-cylinder capacitor (EWCC) model has recently been proposed.[11] The EWCC model captures two key effects: (1) confinement and (2) curvature. The main idea is that counterions form a wire along the axis of small-diameter cylindrical micropores, resulting in a different capacitance regime from that of mesopore structures where curvature effects are also needed for a quantitative description, even though they display smaller mean curvature as compared to micropores. The EWCC model has been shown to fit remarkably well to available experimental data.[11] Although this model sheds light on the anomalous enhancement of capacitance in micropores, many issues remain open. First, it is often thought that micropores are slit-shaped instead of cylindrical, and thus, the EWCC model may not always be applicable, depending on electrode materials synthesis and processing. Second, while the assumption that ions accumulate along the center of electrified micropores seems reasonable from a purely geometric confinement standpoint, details on the confining processes remains largely unproven in the complex electrolyte−electrode interface structure. In fact, because the classical EDL

*Address correspondence to rqiao@clemson.edu, meunierv@ornl.gov.

Received for review January 21, 2010 and accepted March 18, 2010.

Published online April 5, 2010. 10.1021/nn100126w

theories were developed for relatively large pores, the second assumption is against the prediction of the classical EDL theories,[9] which state that counterions accumulate primarily in separate layers near *each* slit wall. However, classical EDL theories are mostly based on the assumption that the ion-distribution is governed only by the electrostatic ion−ion interactions, and thus, predictions based on classical theory may not be accurate. In fact, studies of the EDLs in mesopores (pore size 20−500 Å) and near open surfaces indicate that other factors such as ion hydration effects also play important roles in determining the ion distribution.[12,13] It follows that, in micropores, ions may accumulate predominately in the pore center.

In relation to the above-mentioned issues, many fundamental questions remain to be answered. For example, is the ion distribution primarily governed by the long-range electrostatic ion−ion interactions as in mesopores? What are the hydration characteristics of ions at different positions in electrified micropores, and how and to what extent do they affect the ion distribution? These questions are ideally suited for atomistic simulations. However, most molecular dynamics (MD) simulations of EDLs deal with mesopores,[14−18] and few studies have been reported for the ion distribution in micropores.[19] The limited number of MD studies of micropores focus on neutral pores and the average ion hydration characteristics in such pores.[20,21] The hydration of ions across the pore and how it affects the ion distribution have not been studied extensively.

With the above motivations, here we study the distribution of K^+ ions inside electrified slit-shaped micropores using MD simulations with an emphasis on the role of ion hydration and ion−ion electrostatic interactions on the ion distribution inside the pore. K^+ ions were studied as they are frequently used in aqueous electrolyte-based ECs. The results obtained are then used to construct a new model for EDLs in slit-shaped micropores, which is shown to be capable of predicting the anomalous enhancement of capacitance experimentally observed in micropores.

RESULTS AND DISCUSSION

We investigated the distribution of water molecules and K^+ ions in electrified slit micropores with pore widths (W) ranging from 9.36 to 14.7 Å using MD simulations. In each MD system, a slab of water and ion mixture was enclosed between two charged single graphene layers. The pore width is defined as the separation between the center planes of the two graphene layers. The coordinate system is chosen so that $z = 0$ corresponds to the center plane of the lower wall. The surface charge density (σ) was fixed at -0.055 C/m^2, similar to that measured for microporous activated carbon electrodes immersed in aqueous electrolytes.[6,22] Only counterions (K^+ ions) were included in the pores because co-ions are essentially rejected from these highly charged micropores (or the number of the co-ions is extremely small[20]). Figure 1a shows the water and K^+ ion concentration profiles in negatively charged slit pores with various pore widths. The water distribution inside the slits changes as the width decreases: three layers of water molecules can be identified in slits with $W > 10.7$ Å, while only two layers of water molecules develop in slits with $W \leq 10.7$ Å. In the widest slit studied ($W = 14.7$ Å), the K^+ ion concentration profile resembles that expected from the classical EDL theories to some extent; *i.e.*, counterions accumulate in separate layers near *each* slit wall. However, in slits between 10 and 14.7 Å, K^+ ions accumulate primarily in the central plane of the slits, in disagreement with the classical EDL theories. Finally, in slits with $W = 9.36$ Å, the K^+ ion concentration profile shows one distinct peak near each slit wall, again in qualitative agreement with the classical EDL theories. However, K^+ ions in each peak adjacent to the slit wall is partly dehydrated as inferred from the size of the K^+ ion (shown as circle in Figure 1a) and from the water concentration distribution in the slit. Therefore, the K^+ ions become contact-adsorbed in slits with $W = 9.36$ Å. The low-concentration shoulders in larger pores are also associated with the contact-adsorbed K^+ ions, but unlike in the smallest pore studied, their contributions to the charge storage and to the micropore capacitance are minor.

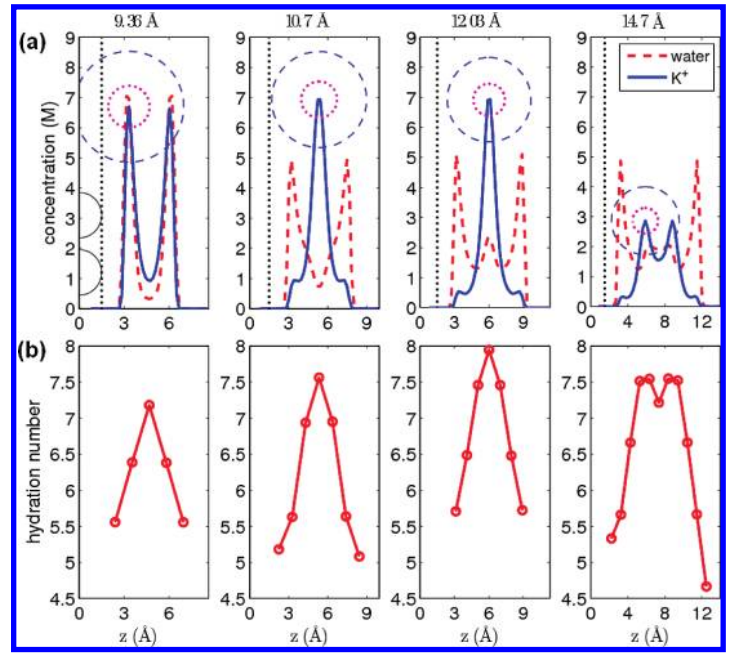

Figure 1. (a) Concentration profiles of water and K^+ ions inside slit pores with various widths. For clarity, the water concentration has been divided by a factor of 30. The concentric circles denote the size of bare and hydrated K^+ ions. The hemicircles in the leftmost figure denote the van der Waals radius of the wall atom, and the dashed line denotes the effective boundary of the lower wall. (b) Hydration number of K^+ ions across slit pores with various widths. All slit walls have the same surface charge density of $\sigma = -0.055$ C/m^2.

To understand the qualitatively different distributions of K^+ ions in different slits, we note that the distri-

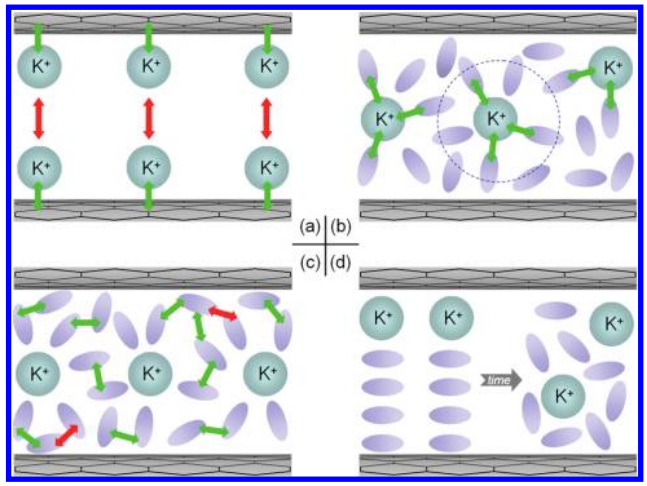

Figure 2. Schematic diagrams of the five factors, as described in the text, governing the distributions of the K^+ counterions in electrified slit-shaped micropores: (a) the long-range electrostatic ion−ion repulsion which drives ions toward the slit walls (factor 1) and the nonelectrostatic ion-slit wall attraction (factor 2), indicated by the red and green double-headed arrows, respectively (color codes also applicable in the following); (b) the hydration of ions (factor 3), which drives ions toward positions to maximize their interactions with the hydration water molecules (the blue dashed circle indicates the primary hydration shell of one ion; compared to the ions in the slit center, the ion near the slit wall has smaller number of hydration water molecules); (c) the interaction between an ion's hydration water molecules with their surrounding water molecules (factor 4); and (d) entropic effects that drive the ordered distribution shown on the left toward a uniform/disordered distribution on the right (factor 5).

bution of counterions in electrified micropores free of co-ions is governed by mainly five factors:[23] (1) the long-range electrostatic ion−ion repulsion, which always drives ions toward the two slit walls (Figure 2a),[24] (2) the nonelectrostatic ion-slit wall attractions that consist of the van der Waals and steric interactions between ion and wall atoms (Figure 2a), (3) the hydration of ions, which drives ions toward positions where they maximize interactions with their hydration water molecules (Figure 2b), (4) the interactions between an ion's hydration water molecules and their surrounding water molecules (Figure 2c),[25] and (5) entropic effects that drive the ion and water inside the slit toward an uniform distribution (Figure 2d). These factors ensure that the free energy of the entire system (ion and water) is minimized at equilibrium. The significance of some of these factors in controlling the EDL structure has been recognized in the EDL literature. For example, electrostatic ion−ion repulsion and the entropy of ions are accounted for in the classical EDL theories,[9] and recent theoretical and modeling work confirms that ion hydration and nonelectrostatic ion−wall interactions cannot be neglected in describing the EDL.[14] However, many details of these factors remain unexplored. First, ion hydration in electrified micropores remains poorly understood. Prior EDL studies were performed within the framework of a primitive model in which water is modeled as Lennard-Jones (LJ) atoms,[26] and thus, ion hydration is not modeled with sufficient details. This limitation is avoided in the more recent atomistic studies of EDLs, but these studies deal with mesopores in which water layers from opposing walls do not interact. This is fundamentally different from the picture illustrated in Figure 1.[14] The hydration of ions in cylindrical micropores has been studied recently due to its relevance to biological ion channels.[20,21] However, how ion hydration across *electrified slit pores* varies as the slit shrinks, which is critical for understanding the EDL capacitance in micropores, has not been explored. Second, the enthalpic and entropic contributions of water to the free energy of the system and their role in controlling the EDL structure are often neglected. Several theoretical models have been proposed to account for these effects,[27,28] but these theories have yet to be applied to EDLs in micropores. Finally, the interplay and relative importance of the above-mentioned five factors in determining the EDLs in micropores have yet to be explored. For example, it is unclear whether the ion−ion electrostatic interactions or the ion hydration effects are the most important factors to determine the ion distribution in slit micropores. Below we show that these unexplored aspects of the EDLs are critical for understanding the different K^+ ion distributions in slits of different widths.

We now examine the role of the above factors in determining the K^+ ion concentration shown in Figure 1a. To examine the role of ion hydration effects, we computed the number of hydration water molecules (hydration number, N_{hyd}) for K^+ ions across various slits (Figure 1b). Following established conventions, the water molecules belonging to the solvation shell of a given ion are defined as those within r_{min1} from the ion, where $r_{min1} = 3.65$ Å corresponds to the first local minimum of the K^+−water pair correlation function.[29] In slits with $W = 14.7$ Å, as a K^+ ion moves away from the slit wall, N_{hyd} increases sharply and reaches a maximum of 7.5 at position 5.8 Å from the slit wall, exactly where the K^+ ion concentration peak is located. In slits with $W = 10.7$ and 12.03 Å, N_{hyd} increases monotonically from the slit wall to the slit center, and the K^+ peak again is located at a position where N_{hyd} is maximized. These results suggest that the ion hydration effects play an important role in determining the K^+ ion distribution in slit pores. For wide pores (or open electrodes) in which accumulation of ions occurs near each slit wall, the ion hydration effects are known to control the location of the concentration peak of small cations.[9] For pore widths in the 10−14 Å range, the ion hydration shells play an even more decisive role in the qualitative breakdown of the classical EDL picture; *i.e.*, they force K^+ ions to form a single layer midway between the slit walls. However, it is interesting that, in pores with $W = 9.36$ Å, the K^+ ion distribution shows an abrupt transition, *i.e.*, K^+ ions form distinct layers near *each* slit wall, although the ion hydration effects should still drive them to the slit center. The most straightforward reason for this transition is that the electrostatic ion−ion repulsions dominate

over the hydration effects for this pore since the ion−ion repulsion strengthens as the slit width decreases.

To elucidate whether the electrostatic ion−ion repulsion is indeed responsible for the formation of separate counterion layer near each wall instead of a single layer in the center of the 9.36 Å pore, it is desirable to compare the difference in electrostatic ion−ion interaction energy in the two different ion configurations. However, since the ion distribution is obtained in only one of these configurations, such a comparison is difficult to perform. Here we adopted a different approach; *i.e.*, we performed PB and MD simulations with different surface charge densities σ to probe the role of electrostatic ion−ion repulsion. If the electrostatic ion−ion repulsion dominates the ion distribution, as σ increases, the counterion concentration near the slit wall will increase more quickly than σ. For example, Figure 3a shows that, as σ increases from −0.007 to −0.055 C/m^2, the maximum ion concentration in the slit scaled by |σ|, *i.e.*, $c_{max}/|\sigma|$, increases by a factor of 3.5 times, according to the classical PB simulations which contain mainly the electrostatic ion−ion repulsion. However, Figure 3b shows that for the same range of σ, MD simulations gave $c_{max}/|\sigma|$ values that are nearly independent of σ. More importantly, at σ = −0.007 C/m^2, our MD system contains only one K^+ ion in each simulation box; thus the electrostatic ion−ion repulsion does not even exist in such an MD system. These results indicate that the electrostatic ion−ion repulsion is not the reason for the contact-adsorption of K^+ ions on the slit wall in slits with W = 9.36 Å.

Since entropic effects are unlikely to cause the distinct K^+ ion peaks near slit walls,[30] we next examine whether nonelectrostatic ion−electrode interactions and interactions between hydration water molecules (*i.e.*, factors 2 and 4 above, see Figure 2) dominate over the ion hydration effects so that K^+ ions prefer to become contact-adsorbed on the slit wall than accumulate in the slit center to maximize their hydration. Specifically, we calculate factors 2, 3, and 4 for the K^+ ions contact-adsorbed on the slit wall and located at the slit center in slits with W = 9.36 Å. To understand the interplay between these factors in larger pores, the same calculations were also performed in a slit with W = 12.03 Å. In all calculations, for an ion located at each position, we computed the interaction energy between the ion and its hydration water molecules or wall atoms, *i.e.*, E_{hyd} and $E_{ion-wall}$. We also computed $E_{water-water}$, the average interaction energy between each of an ion's hydration water molecules with its primary coordination water molecules (*i.e.*, those water molecules within r_{min1} from the hydration water molecule being examined, where r_{min1} = 3.30 Å is the first local minimum of the water−water pair correlation function).[29] The results are summarized in Table 1. In the slit with W = 9.36 Å, we observe that, as a contact-adsorbed K^+ ion moves to the slit center, E_{hyd} decreases by 51.7 kJ/mol. This is consistent with the increase of N_{hyd} shown in Figure 1b and indicates that the ion hydration effects favor the accumulation of ions in the slit center. At the same time, $E_{ion-wall}$ increases by 2.07 kJ/mol, which favors the contact-adsorption of K^+ ions. To test the significance of this effect, we performed a simulation in which the energy well depth, ε_{K^+-wall}, of the Lennard-Jones potential describing the nonelectrostatic ion−wall interactions was reduced to 1/3 of its original value with all other interaction parameters unchanged. The K^+ ion concentration profile in the new simulation was similar to that shown in Figure 1a, indicating that the contribution of the nonelectrostatic ion−wall interactions to the contact-adsorption of K^+ ion on the slit wall is modest. In the same slit, Table 1 also shows that, as a contact-adsorbed K^+ ion moves to the slit center, the average coordination number of its hydration water molecules reduces from 4.29 to 3.96 and the average interaction energy between each of the ion's hydration water molecules with its primary coordination water molecules increases by 5.5 kJ/mol. These results indicate that as a contact-adsorbed K^+ ion moves to the slit center, although it attracts more water molecules toward it to become better hydrated (thus lowering the system energy), it also causes its hydration water molecules to interact with fewer water molecules and therefore to weaken these interactions (thus increasing the system energy).

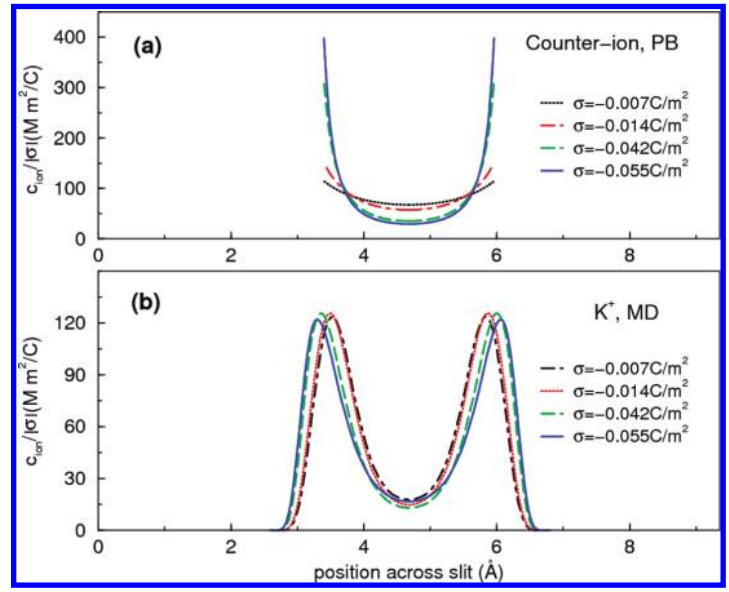

Figure 3. Variation of counterion (K^+ ion) concentration scaled by the slit wall charge density ($c_{ion}/|\sigma|$) in 9.36 Å-wide slits with different surface charge densities. (a) Prediction by the PB equation. The closest approach of the K^+ ion to the slit wall was taken as 3.3 Å. The solution dielectric constant was taken as 3.33, the same as the result of fitting the sandwich capacitor model (in Figures 4 and 5) to the capacitance data obtained from micropores immersed in 6 M KOH electrolytes.[6] (b) Prediction by the MD simulations.

Summarizing the above discussions on the role of electrostatic ion−ion repulsion and nonelectrostatic ion−wall attraction, we conclude that, for slit with W

TABLE 1. Properties of K^+ Ions Located at Different Positions Inside Slit Pores and the Properties of Their Hydration Water Molecules

	in slit with $W = 9.36$ Å		in slit with $W = 12.03$ Å	
	$z_{K+} = 3.30$ Å	$z_{K+} = 4.68$ Å	$z_{K+} = 3.30$ Å	$z_{K+} = 6.02$ Å
interaction energy between a K^+ ions and its hydration water (kJ/mol)	−294.4	−346.1	−296	−336.1
nonelectrostatic (LJ) ion−wall interaction energy (kJ/mol)	−7.4	−5.4	−6.6	−2.0
coordination no. of K^+ ion's hydration water	4.3	4.0	4.2	4.5
interaction energy between each of K^+ ion's hydration water molecules with its coordination water (kJ/mol)	−37.6	−32.1	−35.1	−42.5

= 9.36 Å, the enthalpic effects associated with the interactions between hydration water molecules and their coordinate water dominate over the ion hydration effects and play a critical role in causing the contact-adsorption of K^+ ions on the slit wall. Similar analysis of Table 1's data for slit with $W = 12.03$ Å indicates that these enthalpic effects act *together* with the ion hydration effects to drive the K^+ ions from the slit wall to the slit center. Although the $E_{ion-wall}$ difference works against this explanation, it is only a minor effect for K^+. It is noteworthy that the computed E_{hyd} for K^+ at the pore center for the 12.03 Å slit is close to the experimental value of K^+ in aqueous solution (331.8−338.1 kJ/mol).[31]

To further understand the origins of the opposite role of these enthalpic effects on affecting the K^+ distribution in slits with different widths, we computed the distribution of water around K^+ ions located at the above two positions in the two slit pores. Parts a and b of Figure 4 show the concentration distribution (shown

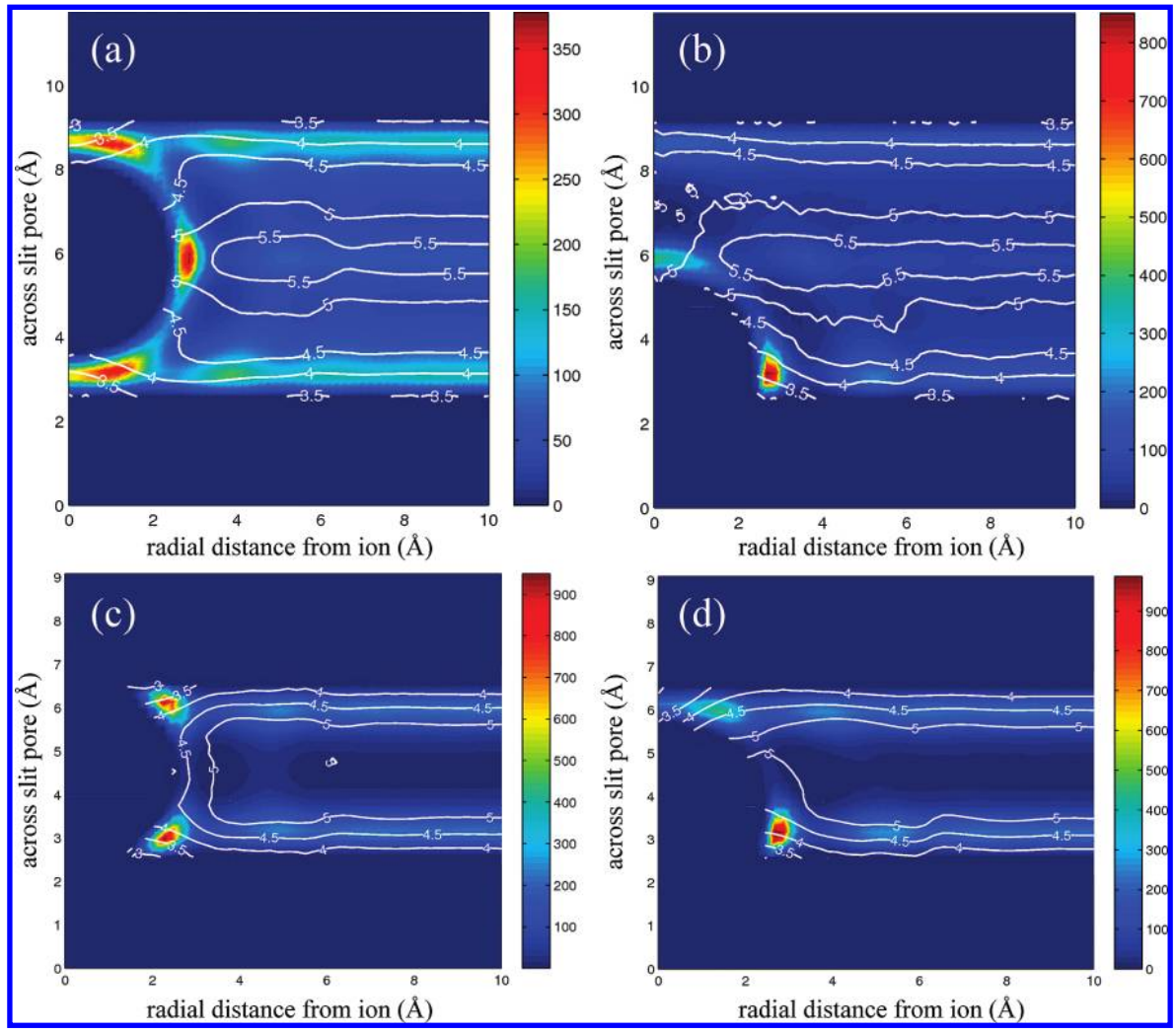

Figure 4. Distribution of water molecules around a K^+ ion located at different positions in slit pores (shown as different colors) and the coordination number of these water molecules (shown as contour lines): (a) K^+ located at $z = 6.03$ Å inside a 12.03 Å-wide slit pore; (b) K^+ located at $z = 3.30$ Å inside a 12.03 Å-wide slit pore; (c) K^+ located at $z = 4.68$ Å inside a 9.36 Å-wide slit pore; (d) K^+ located at $z = 3.30$ Å inside a 9.36 Å-wide slit pore.

with different colors) of water molecules around K^+ ions contact-adsorbed on the slit wall and located at the slit center for a slit with $W = 12.03$ Å. The number of coordination water molecules for the water molecules located at different positions from the K^+ ion is also shown in the same figure as contour lines. We observe that, when a K^+ ion is located at the slit center, its hydration water molecules are distributed near its equator and north/south poles. The hydration water molecules near its equator have a coordination number of 5−5.5, and those near its north/south poles have a coordination number of 3.5−4. As the K^+ ion becomes contact-adsorbed on the slit wall, its hydration water molecules accumulate mainly near its equator, and their coordination number is ~3.5. This different solvation of the hydration water molecules of K^+ ion by other water molecules is consistent with that shown in Table 1 and is a result of the geometrical confinement and the layering of water inside the slit. Specifically, when a K^+ ion is located in the slit center, there is enough space above/below it to accommodate a water layer between its north/south pole and the slit wall, and the hydration water molecules located there are not well solvated since there is no water above/below them. On the other hand, the hydration water molecules near the K^+ ion's equatorial plane are well solvated. When a K^+ ion is contact-adsorbed on the wall of the same slit, its hydration water molecules accumulate primarily near its equator because water concentration there is higher due to the layering of water shown in Figure 1a. Similar to the hydration water molecules near the north/south pole of the K^+ ions located at the slit center, these hydration water molecules are not well solvated. Overall, in slits with $W = 12.03$ Å, the solvation of K^+ ion's hydration water molecules is better when the K^+ ions are located in the slit center than when the K^+ ion is contact-adsorbed. Parts c and d of Figure 4 show the concentration distribution of water molecules around K^+ ions contact-adsorbed on the slit wall and located at the slit center for slit with $W = 9.36$ Å and their coordination number. When a K^+ ion is located in the center of this slit, essentially all its hydration water molecules are distributed near its north and south poles and are not well hydrated (average coordination no. 3.5−4). As the ion becomes contact-adsorbed on the wall, a large fraction of its hydration water molecules is distributed near its equator and it is not well hydrated (average coordination no. ~4). However, because the gap between the K^+ ion and slit wall is wide enough, some of its hydration molecules are distributed near its north pole and have an average coordination number of 4−4.5 due to the high water concentration near the upper slit wall. Therefore, in a slit with $W = 9.36$ Å, the solvation of K^+ ion's hydration water improves when the ion becomes contact-adsorbed.

The above results indicate that, under slit surface charge density relevant to ECs based on microporous carbon electrodes, K^+ ions will form a single layer midway between the opposing slit walls in slit pores between 10 and 14.7 Å wide. Since the micropore capacitance has been measured experimentally, it is desirable to compute the slit pore capacitance directly using MD simulations. A key difficulty associated with the present models for slit pores is that all charges are localized at different points determined by the atomic nuclei instead of being distributed continuously in the space according to the electron densities. This problem needs to be addressed to accurately predict the pore capacitance in pores where opposing pore surfaces share ions.[11] To circumvent this difficulty, here we propose a sandwich capacitance model to describe the capacitance of slit-shaped micropores and fit the experimental capacitance values of microporous carbons.

On the basis of the insight obtained from the above MD simulations, we derive a capacitance formula for a sandwich capacitor formed by a layer of counterions located exactly midway between two electrodes with the same polarity and separated by a pore width of $2b$ (Figure 5). Because the opposing electrodes share the net charge of the counterions, one can approximate the slit capacitor as two capacitors in parallel as shown in Figure 5b. The total capacitance C_{tot} of the system shown in Figure 5b can thus be computed as

$$C_{tot} = 2C_s \tag{1}$$

where C_s is the capacitance of a single capacitor consisting of one electrode and one side of the counterions. Since the electric field lines effectively terminate at the electron cloud of the ions, C_s can be computed using the parallel-plate capacitor model

$$C_s = \varepsilon_r \varepsilon_0 A / d_{eff} \tag{2}$$

where ε_r is the electrolyte dielectric constant, ε_0 the permittivity of a vacuum, A the surface area of the electrode, and d_{eff} the effective separation between the electrode surface and the counterions. Counterions are not simply point charges, and the ionic radii are determined by the location of the charge densities.[11] We stress that the corrections of charge separation by the locations of charge densities are extremely important in producing a reliable capacitance model, especially for micropores. Based on Figure 5b, d_{eff} is equal to $(b - a_0)$, just as described in the EWCC model. However, the present model is derived for parallel plates; *i.e.*, curvature is null. Therefore, the area-normalized total capacitance of the system shown in Figure 5 is obtained as

$$C_{tot}/2A = C_s/A = \varepsilon_r \varepsilon_0 / (b - a_0) \tag{3}$$

As can be seen in Figure 6, for the microporous activated carbon electrodes immersed in 6 M KOH electrolyte solution, the area-normalized capacitance has been found to increase from ~6 to ~12 μF/cm^2 as the mean pore size of the electrode decreases from 14.5 to 10.6

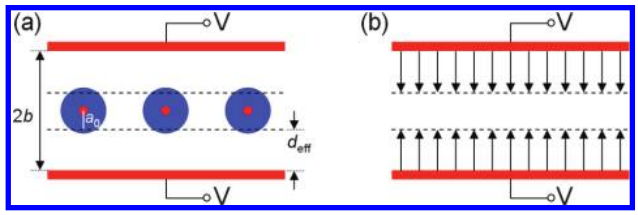

Figure 5. (a) Schematic of a sandwich capacitor formed by a layer of counterions located exactly midway between two electrodes with the same polarity and separated by $W = 2b$. (b) The equivalent system shown with the electric field lines. The locations of the dashed lines indicate the effective ion radius a_0 of the counterions, which is dictated by the spread of electron cloud (ref 11). The effective separation between the electrode surface and the counterions is d_{eff}.

Å.[6] This pore size range is in rough agreement with that found by our MD simulations where fully hydrated K^+ ions accumulate primarily in the central plane of the slit pores. Using the sandwich capacitance model given by eq 3, we were able to fit the experimental data with an R^2 value of 0.926, reproducing the experimental trend and giving two fitting parameters of $\varepsilon_r = 3.33 \pm 0.57$ and $a_0 = 2.65 \pm 0.54$ Å. That the ε_r value is larger than the vacuum value of unity implies that the electrolyte ions are hydrated in the pore width range studied, which is supported by Figure 1a. The ε_r value is smaller than those in the Helmholtz layer near isolated electrodes (typically less than 10)[2] and may originate from the extreme confinement of water in the micropores.[32,33] Even with the standard error of 0.54 Å considered, the a_0 value is not in very good agreement with the ion radius of K^+ (1.38 Å).[34] A similar fit realized using the EWCC model yields a R^2 value of 0.921 as

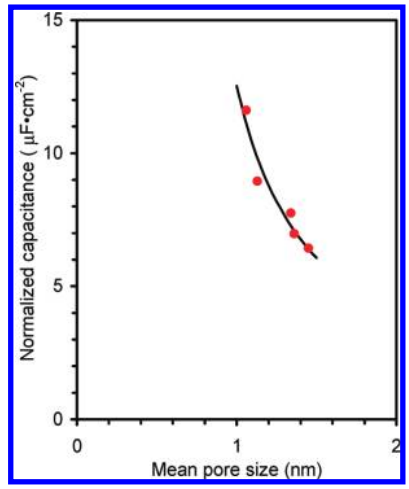

Figure 6. Experimental data (solid dots) in ref 6 of microporous activated carbon electrode materials in a 6 M aqueous KOH electrolyte fit with the sandwich capacitance model (solid curve) shown in eq 3.

well. However, in this case, a_0 (1.64 Å) is found to be much closer to the ionic radius of K^+. This indicates that confinement effects (use of a_0 explicitly) are key in a qualitative description of the capacitance behavior for small pores (*i.e.*, sharp increase with decreasing width), as is described in detail here. However, our fits also indicate that curvature effects are very important for a quantitative description of the capacitance value, especially when pore geometry is closer to that of a cylinder rather than that of a slit.

CONCLUSION

In summary, we have studied the distribution of K^+ ions in electrified slit-shaped micropores with pore widths ranging from 9.36 to 14.7 Å using MD simulations. We have examined in detail the five main factors that govern the distribution of K^+ ions in electrified micropores: (1) the long-range electrostatic ion−ion repulsion, which always drives ions toward the two slit walls, (2) the nonelectrostatic ion-slit wall attractions, (3) the hydration of ions, which drives ions toward positions where they maximize interactions with their hydration water molecules, (4) the interactions between an ion's hydration water molecules and their surrounding water molecules, and (5) entropic effects that drive the ion and water inside the slit toward an uniform distribution. The highlight of our results is that K^+ ions form a well-hydrated single layer in the center of negatively charged slit pores with pore width between 10 and 14.7 Å. Such an ion distribution differs qualitatively from the prediction by the classical EDL theories and is caused primarily by the ion hydration effects. In slits with a width of 9.36 Å, the K^+ ions form separate layers near each slit wall. We found that the electrostatic ion−ion repulsion plays only a minor role in such a transition. Instead, the enthalpic effects associated with the interactions between the hydration water molecules of the K^+ ion with their surrounding water molecules were found to lead to this interesting behavior. Based on the K^+ ion distribution observed in electrified slits with 10 Å $< W <$ 14.7 Å, we proposed a sandwich model to predict the scaling of the slit pore capacitance as a function of its pore width. This model is shown to be capable of predicting the anomalous enhancement of capacitance that has been experimentally observed in micropores with similar widths. However, curvature effects are indispensable for a quantitative description of the experimental capacitance values, further implying that the microporous carbons in ref 6 have a local pore geometry that are closer to a cylinder shape rather than that of a slit.

METHODS

The MD simulations were performed using a customized version of MD package Gromacs.[35] For each electrified slit pore, we placed small partial charges on a plane at a position 0.7 Å away from the slit surface to produce the desired surface charge density.[36] The number of K^+ ions inside the slits was chosen to ensure the overall electroneutrality of the system.[26] To obtain an MD system in which the chemical po-

tential of water molecules inside the slit is equal to that in bulk solution, we first connected the slit to a large water bath with one end exposed to vacuum and performed NVT simulations ($T = 300$ K) for 3−10 ns for the water molecules inside the slit to allow for complete equilibration. During these simulations, "ghost" gate atoms, which do not interact with water molecules, were placed at the entrance/exit of the slit pore to prevent K^+ from leaving the slit. Next, the water bath was removed, and periodical boundary conditions were enforced in all three directions. To remove the periodicity in the direction normal to the slit wall, the simulation box size in this direction was extended to be 5 times that of the slit width, and the slab-PME method was used to compute the electrostatic interactions. The simulations were performed for 100 ns, and the trajectories were saved every 10 ps for analysis. The force fields for water and K^+ ions was taken from ref 29 and the force field for carbon atoms were taken from the sp^2 carbon of the force fields in ref 37. Other simulation details can be found in ref 13.

Acknowledgment. The authors thank the Clemson-CCIT office for providing computer time. The Clemson authors acknowledge support from the NSF under Grant No. CBET-0756496. R.Q. was partly supported by an appointment to the HERE program for faculty at the Oak Ridge National Laboratory (ORNL) administered by ORISE. The authors at ORNL gratefully acknowledge the support from the Laboratory Directed Research and Development Program of ORNL and from U.S. Department of Energy under Contract No. DEAC05-00OR22725 with UT-Battelle, LLC at ORNL.

REFERENCES AND NOTES

1. US Department of Energy. Basic Research Needs for Electrical Energy Storage: Report of the Basic Energy Sciences Workshop on Electrical Energy Storage, 2007.
2. Conway, B. E. *Electrochemical Supercapacitors: Scientific Fundamentals and Technological Applications*; Kluwer Academic/Plenum: New York, 1999.
3. Miller, J. R.; Simon, P. Electrochemical Capacitors for Energy Management. *Science* **2008**, *321*, 651–52.
4. Simon, P.; Gogotsi, Y. Materials for Electrochemical Capacitors. *Nat. Mater.* **2008**, *7*, 845–854.
5. Zhang, L. L.; Zhao, X. S. Carbon-Based Materials as Supercapacitor Electrodes. *Chem. Soc. Rev.* **2009**, *38*, 2520–2531.
6. Lota, G.; Centeno, T. A.; Frackowiak, E.; Stoechkli, F. Improvement of the Structural and Chemical Properties of a Commercial Activated Carbon for its Application in Electrochemical Capacitors. *Electrochim. Acta* **2008**, *53*, 2210–2216.
7. Chmiola, J.; Yushin, G.; Gogotsi, Y.; Portet, C.; Simon, P.; Taberna, P. L. Anomalous Increase in Carbon Capacitance at Pore Sizes Less than 1 Nanometer. *Science* **2006**, *313*, 1760–1763.
8. Largeot, C.; Portet, C.; Chmiola, J.; Taberna, P.-L.; Gogotsi, Y.; Simon, P. Relation between the Ion Size and Pore Size for an Electric Double-Layer Capacitor. *J. Am. Chem. Soc.* **2008**, *130*, 2730–2731.
9. Israelachvili, J. *Intermolecular and Surface Forces*; Academic Press: New York, 1992.
10. Bard, A. J.; Faulkner, L. R. *Electrochemical Methods: Fundamentals and Applications*, 2nd ed.; John Wiley & Sons: New York, 2001.
11. Huang, J.; Sumpter, B. G.; Meunier, V. A Universal Model for Nanoporous Carbon Supercapacitors Applicable to Diverse Pore Regimes, Carbon Materials, and Electrolytes. *Chem.—Eur. J.* **2008**, *14*, 6614–6626.
12. Cui, S. T.; Cochran, H. D. Molecular Dynamics Simulation of Interfacial Electrolyte Behaviors in Nanoscale Cylindrical Pores. *J. Chem. Phys.* **2002**, *117*, 5850–5854.
13. Qiao, R.; Aluru, N. R. Atomistic Simulation of KCl Transport in Charged Silicon Nanochannels: Interfacial Effects. *Colloids Surf. A* **2005**, *267*, 103–109.
14. Freund, J. B. Electro-osmosis in a Nanometer-Scale Channel Studied by Atomistic Simulation. *J. Chem. Phys.* **2002**, *116*, 2194–2200.
15. Qiao, R.; Aluru, N. R. Ion Concentrations and Velocity Profiles in Nanochannel Electroosmotic Flows. *J. Chem. Phys.* **2003**, *118*, 4692–4701.
16. Dufreche, J. F.; Marry, V.; Malikova, N.; Turq, P. Molecular Hydrodynamics for Electroosmosis in Clays: From Kubo to Smoluchowski. *J. Mol. Liq.* **2005**, *118*, 145–153.
17. Wang, M.; Liu, J.; Chen, S. Similarity of Electroosmotic Flows in Nanochannels. *Mol. Simul.* **2007**, *33*, 239–244.
18. Chen, Y. F.; Ni, Z. H.; Wang, G. M.; Xu, D. Y.; Li, D. Y. Electroosmotic Flow in Nanotubes with High Surface Charge Densities. *Nano Lett.* **2008**, *8*, 42–48.
19. Yang, K. L.; Yiacoumi, S.; Tsouris, C. Monte Carlo Simulations of Electrical Double-Layer Formation in Nanopores. *J. Chem. Phys.* **2002**, *117*, 8499–8507.
20. Shao, Q.; Zhou, J.; Lu, L. H.; Lu, X. H.; Zhu, Y. D.; Jiang, S. Y. Anomalous Hydration Shell Order of Na^+ and K^+ inside Carbon Nanotubes. *Nano Lett.* **2009**, *9*, 989–994.
21. Song, C.; Corry, B. Intrinsic Ion Selectivity of Narrow Hydrophobic Pores. *J. Phys. Chem. B* **2009**, *113*, 7642–7649.
22. We also investigated the ion distribution in slit pores with the same widths studied here but with surface charge densities of ± 0.014 and ± 0.083 C/m^2. The ion distribution across these slit pores shows the same trend as reported here.
23. If the electronic degree of freedom of the slit wall is also accounted for, additional factors will be at play. However, this is outside the scope of this work.
24. As pointed out in ref 9, the electrostatic ion-slit wall interactions play no role in determining the ion distribution when co-ions are completely rejected from the slit pore.
25. In principle, the interactions between the ion's hydration water and pore wall atoms should also be considered. However, these interactions are not detailed here because such interactions are much weaker than the water−water interactions and show little change as the ion moves across the microslits considered here.
26. Lo, W. Y.; Chan, K. Y.; Lee, M.; Mok, K. L. Molecular Simulation of Electrolytes in Nanopores. *J. Electroanal. Chem.* **1998**, *450*, 265–272.
27. Lamperski, S.; Outhwaite, C. W. A Non-Primitive Model for the Electrode/Electrolyte Interface Based on the Percus-Yevick Theory. Analysis of the Different Molecular Sizes, Ion Valences and Electrolyte Concentrations. *J. Electroanal. Chem.* **1999**, *460*, 135–143.
28. Burak, Y.; Andelman, D. Hydration Interactions: Aqueous Solvent Effects in Electric Double Layers. *Phys. Rev. E* **2000**, *62*, 5296–5312.
29. Lee, S. H.; Rasaiah, J. C. Molecular Dynamics Simulation of Ion Mobility. 2. Alkali Metal and Halide Ions Using the SPC/E Model for Water at 25 °C. *J. Phys. Chem.* **1996**, *100*, 1420–1425.
30. The potential of mean force (PMF) of a K^+ ion located at the peak adjacent to the slit was found to be 2.04 k_BT (k_B is the Boltzmann constant, $T = 300$ K) lower than that at the slit center. Since this PMF difference is larger than k_BT, the entropic effects alone are unlikely to cause K^+ ions to accumulate in the peaks adjacent to the slit wall.
31. Frese, K. W., Jr. Calculation of Gibbs Hydration Energy with the Ion-Dielectric Sphere Model. *J. Phys. Chem.* **1989**, *93*, 5911–5916.
32. Palmer, L. S.; Cunliffe, A.; Hough, J. M. Dielectric Constant of Water Films. *Nature* **1952**, *170*, 796.
33. Dzubiella, J.; Hansen, J.-P. Electric-Field-Controlled Water and Ion Permeation of a Hydrophobic Nanopore. *J. Chem. Phys.* **2005**, *122*, article no. 234706.
34. Marcus, Y. A Simple Empirical Model Describing the Thermodynamics of Hydration of Ions of Widely Varying Charges, Sizes, and Shapes. *Biophys. Chem.* **1994**, *51*, 111–127.

35. Lindahl, E.; Hess, B.; van der Spoel, D. GROMACS 3.0: a Package for Molecular Simulation and Trajectory Analysis. *J. Mol. Model.* **2001**, *7*, 306–317.
36. Meunier, V.; Kalinin, S. V.; Shin, J.; Baddorf, A. P.; Harrison, R. J. Quantitative Analysis of Electronic Properties of Carbon Nanotubes by Scanning Probe Microscopy: from Atomic to Mesoscopic Length Scales. *Phys. Rev. Lett.* **2004**, *93*, article no. 246801.
37. Cornell, W. D.; Cieplak, P.; Bayly, C. I.; Gould, I. R.; Merz, K. M.; Ferguson, D. M.; Spellmeyer, D. C.; Fox, T.; Caldwell, J. W.; Kollman, P. A. A Second Generation Force Field for the Simulation of Proteins, Nucleic Acids, and Organic Molecules. *J. Am. Chem. Soc.* **1995**, *117*, 5179–5197.